PAPER: Biological modelling and information

Optimal resource diffusion for suppressing disease spreading in multiplex networks

Xiaolong Chen[1,2], Wei Wang[2,3,6], Shimin Cai[1,2], H Eugene Stanley[4] and Lidia A Braunstein[4,5]

[1] Web Sciences Center, University of Electronic Science and Technology of China, Chengdu 611731, People's Republic of China
[2] Big data research center, University of Electronic Science and Technology of China, Chengdu 610054, People's Republic of China
[3] Cybersecurity Research Institute, Sichuan University, Chengdu 610065, People's Republic of China
[4] Center for Polymer Studies and Department of Physics, Boston University, Boston, MA 02215, United States of America
[5] Instituto de Investigaciones Físicas de Mar del Plata (IFIMAR)-Departamento de Física, Facultad de Ciencias Exactas y Naturales, Universidad Nacional de Mar del Plata-CONICET, Funes 3350, (7600) Mar del Plata, Argentina
E-mail: wwzqbx@hotmail.com

Abstract. Resource diffusion is a ubiquitous phenomenon, but how it impacts epidemic spreading has received little study. We propose a model that couples epidemic spreading and resource diffusion in multiplex networks. The spread of disease in a physical contact layer and the recovery of the infected nodes are both strongly dependent upon resources supplied by their counterparts in the social layer. The generation and diffusion of resources in the social layer are in turn strongly dependent upon the state of the nodes in the physical contact layer. Resources diffuse preferentially or randomly in this model. To quantify the degree of preferential diffusion, a bias parameter that controls the resource diffusion is proposed. We conduct extensive simulations and find that the preferential resource diffusion can change phase transition type of the

[6] Author to whom any correspondence should be addressed.

fraction of infected nodes. When the degree of interlayer correlation is below a critical value, increasing the bias parameter changes the phase transition from double continuous to single continuous. When the degree of interlayer correlation is above a critical value, the phase transition changes from multiple continuous to first discontinuous and then to hybrid. We find hysteresis loops in the phase transition. We also find that there is an optimal resource strategy at each fixed degree of interlayer correlation under which the threshold reaches a maximum and the disease can be maximally suppressed. In addition, the optimal controlling parameter increases as the degree of inter-layer correlation increases.

Keywords: agent-based models, epidemic modelling, network dynamics, random graphs, networks

Contents

1. Introduction

Epidemic spreading is an important topic in complex systems theory [1] and much research on its underlying dynamics has been conducted in recent years. Although a strong focus has been on the theoretical analysis of epidemic spreading [2, 3], research has also included the control and prediction of disease outbreaks [4, 5], the spread of rumors [6, 7], and the propagation of computer viruses [8, 9]. As more and more infectious diseases such as Severe acute respiratory syndrome (SARS) [10], Ebola virus [25] have brought disasters to humans, how to constrain the global pandemics has been one of most important and pressing challenges. In recent years, many immunization strategies have been proposed for containing and limiting epidemics. Traditional immunization strategies fall into two categories. The first category includes topology-based strategies, such as random immunization [11, 12], targeted immunization [13–15], acquaintance immunization [16], and graph partitioning [17]. Recent successes have used a targeted destruction of the potential transmission network before an outbreak

occurs. 'Super-blockers' are identified and immunized to efficiently break network connectivity [18]. The second category includes those that focus on the dynamics of the diffusion of information about the disease, such as information-driven vaccination patterns [19–21]. Another research topic in epidemic spreading is developing optimal strategies of deploying limited resources such that the epidemic outbreak can be most efficiently suppressed [22–24].

Most research on immunization strategies and optimal resource deployment assumes that available resources are fixed, static, and exist independent of the dynamic epidemic process, but in real-world scenarios the amount of such available resources as drugs, medical personnel, and financial support are strongly affected by the evolution of the disease. For example, a pandemic, e.g. the Ebola virus disease [25], can quickly become an enormous economic burden to a region [26], and even after the disease has been brought under control the economic recovery of the region is slow [27]. Much recent research has examined how dynamic changes in resources affect the dynamics of epidemic spreading. Some research has focused on public resources [28–30]. For example, [28] describes how resource constraints caused by the outbreak of disease affect the dynamics of the epidemic. They assume that healthy individuals in the system provide the needed resources, and that the number of these healthy individuals decreases as the infection rate increases. [30] finds that there is a critical amount of invested public resource needed to constrain the spread of a disease, and when that amount is larger than the critical value, the disease can be suppressed. If it is not, the fraction of infected individuals can quickly increase. Other researchers assume that real-world infected individuals cannot always receive public resources and must seek help from friends in their social circles, and that understanding this phenomenon is important in controlling an epidemic. [31] examines how social supports affect epidemic spreading in a double-layer multiplex network in which one layer is the pattern of resource allocation and the other is of epidemic spreading. They find a hybrid transition in the fraction of infected nodes that exhibits properties of both continuous and discontinuous phase transitions. For the continuous (discontinuous) phase transition, the fraction of infected nodes versus the transmission probability is smooth (abrupt) when the network size is extremely large.

Although the above literature examines the dynamic evolution of resources and their influence on epidemic spreading, it overlooks the phenomenon of resource diffusion among individuals. Such resources as economic wealth constantly flow among individuals. An important topic for research involves the so-called 'Matthew effect' [32] in which the flow of economic wealth tends to make the rich richer. This is relevant because infected individuals with wealth tend to receive better treatment and have a higher probability of recovering than those without.

To investigate the properties of resource diffusion and how it impacts disease spreading, we examine its multiplex structure [31, 33, 34]. We form a two-layer multiplex network of N nodes. Each node in one layer has a counterpart in the other layer. The structure of the two layers can differ. For example, a person may have one group of friends with whom they have regular face-to-face contact and another group of friends in the on-line world [35].

Here we investigate how resource diffusion affects the dynamics of epidemic spreading in two-layer multiplex networks. We assume that resources diffuse among nodes

in the social layer $\mathcal{S}$, and that the disease spreads in the physical contact layer $\mathcal{C}$. Because the diffusion of resources among nodes in layer $\mathcal{S}$ can be either preferential or random, we introduce a bias parameter α that controls the diffusion. When the nodes are healthy they can generate new resources. The recovery of infected nodes in layer $\mathcal{C}$ depends on the resources of their counterparts in layer $\mathcal{S}$. Through simulations we find that the preferential diffusion of resources can change the phase transition type of the fraction of infected nodes at the steady state $\rho(\infty)$. When the degree of interlayer correlation r is below a critical value r_c, and the initial fraction of infected nodes $\rho(0)$ is large, i.e. $\rho(0) = 0.99$, the phase transition $\rho(\infty)$ changes from two continuous phase transitions to a single continuous transition as α increases. In addition, there are two hysteresis loops accompanying the two phase transitions when α is below a critical value α_c, and one hysteresis loop when $\alpha > \alpha_c$. When $r > r_c$, the phase transition of $\rho(\infty)$ changes from multiple (when α is too large or too small) to discontinuous, and then to hybrid, with a initial continuous transition followed by a discontinuous transition. There is always a single hysteresis loop. Note that there is an optimal strategy of resource diffusion under which the disease can be most effectively suppressed, and the threshold reaches a maximum.

2. Model

2.1. The social-contact double layer network

We model the coupling of the dynamics of disease spreading and resource diffusion in a double-layer multiplex network. Each individual has links with colleagues or coworkers in the physical contact layer and also with friends in the social relation layer. We construct the double-layer multiplex network model using the uncorrelated configuration model to independently generate layers $\mathcal{S}$ and $\mathcal{C}$ [36]. These two subnetworks have the same number of nodes N, and there is a one-to-one correspondence between nodes in the two layers. Each layer also has its own internal structure. In an uncorrelated double-layer network, the node degrees in the first layer are independent of the nodes degrees in the second. Thus a high-degree node in the first layer does not necessarily have a corresponding high-degree counterpart in the second. In contrast, in a correlated double-layer network the node degrees in one layer are somewhat dependent on the node degrees in the other layer. Quantitatively, we use the Spearman rank correlation coefficient r [37, 38] in which $r \in [-1, 1]$ to characterize the degree correlation between the two layers. For example, when $r > 0$ the two layers are positively correlated. A larger r value indicates a higher probability that a high-degree node in the first layer matches a high-degree node in the second layer. In contrast, when $r < 0$ the two layers are negatively correlated. A smaller value of r indicates a higher probability that a high-degree node in the first layer matches a low-degree node in the second layer. The topological structure of the two layers are encoded in the two adjacency matrices $A^{\mathcal{S}} = \{a_{ij}^{\mathcal{S}}\}$ and $A^{\mathcal{C}} = \{a_{ij}^{\mathcal{C}}\}$, respectively. If nodes i and j are connected by a link in layer $\mathcal{S}$ ($\mathcal{C}$), $a_{ij}^{\mathcal{S}} = 1$ ($a_{ij}^{\mathcal{C}} = 1$), otherwise $a_{ij}^{\mathcal{S}} = 0$ ($a_{ij}^{\mathcal{C}} = 0$).

2.2. Coupling disease spreading and resource diffusion

To examine how resource diffusion affects epidemic spreading we propose a resource-based susceptible-infected-susceptible (rSIS) model to describe the epidemic spreading in layer $\mathcal{C}$. In the rSIS model, each node can be either susceptible or infected. The recovery process of the infected nodes depends on the resources of their counterparts in layer $\mathcal{S}$. We denote $\rho_i(t)$ to be the probability that node i is infected at time t, and $\rho(t)$ to be the fraction of infected nodes at t, which is determined by averaging over the infection probability of all nodes

$$\rho(t) = \frac{1}{N} \sum_{i=1}^{N} \rho_i(t). \tag{1}$$

Here $\rho(\infty)$ is the fraction of infected nodes when $t \to \infty$.

We first randomly select a fraction of $\rho(0)$ nodes to be seeds (infected nodes) and leave the remaining nodes in the susceptible state. At each time step the infected nodes transmit the disease to susceptible neighbors at an infection rate β. The recovery of infected nodes is dependent upon resources supplied by their counterparts in layer $\mathcal{S}$.

Because resources can promote the recovery of infected nodes, we consider that when a node in layer $\mathcal{S}$ has greater resources the corresponding node in layer $\mathcal{C}$ will have a higher recovery rate. We denote $\mu_i(t)$ the recovery rate of node i at time t, which is a monotonically increasing function of the resource quantity owned by the counterpart of i in layer $\mathcal{S}$. Note that $\mu_i(t)$ is a constant value for all nodes in the classical SIS model. Specifically, $\mu_i(t)$ can be expressed

$$\mu_i(t) = 1 - (1 - \mu_0)^{\omega_i(t)}, \tag{2}$$

where μ_0 is the basic recovery rate, which we here fix at $\mu_0 = 0.1$, and $\omega_i(t)$ is the accumulated resources of the counterpart of node i in layer $\mathcal{S}$ at time t.

The resource diffusion in layer $\mathcal{S}$ is dependent upon the state of nodes in layer $\mathcal{C}$. At each time step, if node i in layer $\mathcal{C}$ remains in the S state, the corresponding node in layer $\mathcal{S}$ generates a new unit of resource. At the same time, depending on the sign of α, it preferentially transfers one unit of resource to one of its neighbors (the target neighbor). Note that the target neighbor is chosen independent of its state, but the target node does not transmit resources to neighbors if it is not in the S state.

We denote $\phi_{i \to j}$ the resource transfer probability from node i to j and assume that this transfer probability is related to the degree of j. Then $\phi_{i \to j}$ is

$$\phi_{i \to j} = \frac{(a_{ij}^{\mathcal{S}} + \delta_{ij}) k_j^{\alpha}}{\sum_{\ell} a_{\ell i}^{\mathcal{S}} k_{\ell}^{\alpha} + k_i^{\alpha}}, \tag{3}$$

where $\delta_{ij} = 1$ if $i = j$, otherwise $\delta_{ij} = 0$. The parameter α allows us to tune the degree of preference. When $\alpha > 0$, $\phi_{i \to j}$ is positively related to the degree of j and a high-degree neighbor has a high probability of being selected, but when $\alpha = 0$, every neighbor of node i has the same probability of being selected. Note that when $i = j$ node i retains the unit of resource during the current time step. The resources $\sigma_j(t)$ that node j acquires from healthy neighbors at time t, can be written

$$\sigma_j(t) = \sum_{i=1}^{N} a_{ij}^{\mathcal{S}} \phi_{i \to j} (1 - \rho_i(t)). \tag{4}$$

When node i in layer $\mathcal{C}$ is in the I state, the corresponding node in layer $\mathcal{S}$ does not generate a new resource unit nor does it transfer a resource unit to its neighbors. The accumulated resources of the counterpart of node i in layer S are consumed. For simplicity, we assume that infected nodes consume the all resources of their counterparts. Thus $\omega_i(t)$ returns to 0 at the current time step. The susceptible nodes store the resources to distribute to neighbors or recover when they are infected in the following time.

We use synchronous updating [2] to simulate the coupled dynamic process of disease spreading and resource diffusion. At each time step with a probability $\beta \Delta t$ a susceptible node is infected by one of its infected neighbors. Simultaneously, infected nodes recover with a probability $\mu_i(t)\Delta t$, where $i = 1...N$. We set a time step $\Delta t = 1$ and run each simulation sufficiently long to ensure that the system enters a steady state in which either no nodes are infected or the number of infected nodes fluctuates within a small range.

3. Simulation results for uncorrelated networks

Here we examine how preferential resource diffusion affects disease spreading in uncorrelated double-layer networks. We focus on networks with a heterogeneous degree distribution because many networked systems in both nature and technological applications are complex and have a heterogeneous degree distribution [39, 40]. We use an uncorrelated configurational model [36, 41] to build a double-layer network in which the degree distribution is $P(k) \sim k^{-\gamma_{\mathcal{S}}}$ for layer $\mathcal{S}$ and is $P(k) \sim k^{-\gamma_{\mathcal{C}}}$ for layer $\mathcal{C}$, where $\gamma_{\mathcal{S}}$ and $\gamma_{\mathcal{C}}$ are the power exponents. We fix both values of the power exponential at $\gamma_{\mathcal{S}} = \gamma_{\mathcal{C}} = 2.2$, and both $\gamma_{\mathcal{S}}$ and $\gamma_{\mathcal{C}}$ are denoted to γ if there is no other special statement. To avoid degree correlations between two layers, each layer is made independent. Because the simulations are time consuming, we set the system size to $N = N_{\mathcal{S}} = N_{\mathcal{C}} = 5000$. For the maximum degree we use the structural cut-off $k_{\max} \sim \sqrt{N}$ [42] and set the minimum degree at $k_{\min} = 2$ [43]. To determine the epidemic threshold, we use a susceptibility measurement [44, 45]

$$\chi = N \frac{\langle \rho(\infty)^2 \rangle - \langle \rho(\infty) \rangle^2}{\langle \rho(\infty) \rangle}, \tag{5}$$

where $\langle \cdots \rangle$ is the ensemble averaging, and χ exhibits peaks at the transition points if they exist.

We first examine the fraction of infected nodes at the steady state $\rho(\infty)$ as a function of β with a small fraction of seeds $\rho(0) = 0.01$ and a large fraction of seeds $\rho(0) = 0.99$. Figures 1(a), (d) and (g) show the results for three typical values $\alpha = -2.0$, -1.0, and 1.0, respectively. We find the following:

   (i) The value of $\rho(\infty)$ increases continuously with β for the three values of α when $\rho(0) = 0.01$ and $\rho(0) = 0.99$.

(ii) When $\alpha = -2.0$ and $\alpha = -1.0$, there are two phase transitions [46, 47] of $\rho(\infty)$ for $\rho(0) = 0.99$ and a single phase transition for $\rho(0) = 0.01$ (see figures 1(a) and (d)). When $\alpha = 1.0$ there is a single phase transition for both $\rho(0) = 0.01$ and $\rho(0) = 0.99$ (see figure 1(g)). Figures 1(b), (e) and (h) show peaks of χ that are transition points for $\rho(0) = 0.99$ (blue squares) and $\rho(0) = 0.01$ (red line).

(iii) As description of the model, we know that the spreading dynamics has strong nonlinearity and memory characteristics, the interplay between these two characteristics may induce the emergence of hysteresis loop [48, 49]. Such as is the case of magnetic materials in the presence of an external field, when you change the orientation of the field. The plot indicates two hysteresis loops when $\alpha = -2.0$ and $\alpha = -1.0$, and a single hysteresis loop when $\alpha = 1.0$. Following the definitions in [50], here we denote by β_{inv} the invasion threshold when $\rho(0) = 0.01$, and β_{per} the persistence threshold when $\rho(0) = 0.99$. In addition, we denote β_{per}^I and $\beta_{\mathrm{per}}^{II}$ the first and the second invasion (persistence) thresholds.

We next examine the underlying mechanism of the hysteresis loop. Figures 1(c), (f) and (i) show the ensemble average recovery rate at the steady state $\langle \mu(\infty) \rangle = 1/N \sum \mu_i(\infty)$, for $\alpha = -2.0$, $\alpha = -1.0$, and $\alpha = 1.0$, respectively. We find that for these values of α, prior to the threshold the average recovery rate is $\langle \mu(\infty) \rangle = 1.0$ and after the threshold it decreases continuously with β. When the spreading process begins with a low fraction of seeds, i.e. $\rho(0) = 0.01$, the recovery rate is higher than when there is a larger initial fraction of seeds, i.e. $\rho(0) = 0.99$ (see figures 1(c), (f) and (i)). This is because when $\rho(0)$ is small the fraction of susceptible nodes $(1 - \rho(0))$, is sufficiently high to generate a large number of resources. A lower recovery rate for $\rho(0) = 0.99$ delays the recovery of infected nodes and increases the infection rate $\lambda = \beta / \langle \mu(\infty) \rangle$ [1]. Thus the disease breaks out at a lower threshold when $\rho(0) = 0.99$, and the value of $\rho(\infty)$ is larger than when $\rho(0) = 0.01$. Consequently there is a hysteresis loop. In addition, when $\alpha = -2.0$ and $\alpha = -1.0$ the two curves of $\langle \mu(\infty) \rangle$ for $\rho(0) = 0.99$ and $\rho(0) = 0.01$ overlap at some value of β that separates the parameter space of β into two regions. Thus there are two hysteresis loops in the separated regions.

To determine how preferential resource diffusion affects the dynamics of disease spreading, we examine $\rho(\infty)$ as a function of β and $\alpha \in [-2.0, 2.0]$. Figures 2(a) and (b) show the phase diagrams with initial conditions $\rho(0) = 0.01$ and $\rho(0) = 0.99$, respectively, and figure 2(c) shows the difference between values of $\rho(\infty)$ in figures 2(a) and (b). Note that $\rho(\infty)$ increases continuously with β at each fixed α. In addition, when $\rho(0) = 0.01$ there is a single phase transition with one threshold β_{inv} (circles in figure 2(a)). When $\rho(0) = 0.99$ there is a critical α_c value below which there is a double phase transition with two transition points β_{per}^I and $\beta_{\mathrm{per}}^{II}$ (circles in figure 2(b)). Note that the thresholds in figures 2(a) and (b) are the peaks of susceptibility χ. We also find that when β is fixed, $\rho(\infty)$ first decreases and then increases with α when β is large, i.e. $\beta > \beta_{\mathrm{inv}}$ ($\beta > \beta_{\mathrm{per}}^I$, if there are two thresholds). We find that there is an optimal value of α_{opt}, at which the invasion and persistence thresholds are maximized, and the disease is greatly suppressed. Note also that the invasion threshold β_{inv} and persistence threshold β_{per}^I (circles in (a) and (b)) have peak values at $\alpha_{\mathrm{opt}} = -1.0$, which indicates
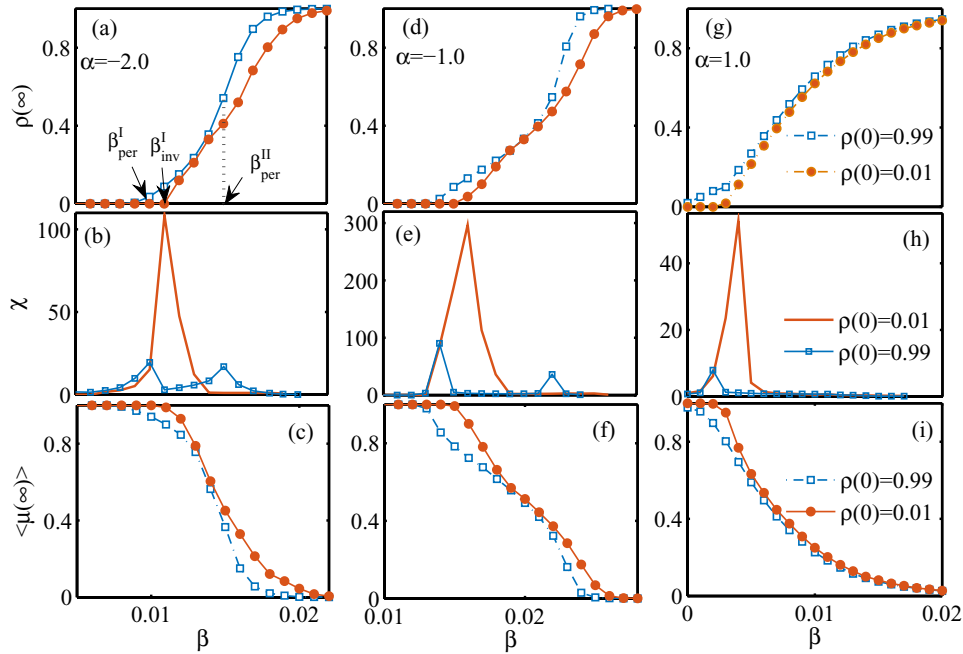
Figure 1. Influence of preferential resource diffusion on disease spreading. Fraction of infected nodes $\rho(\infty)$ as a function of β for $\alpha = -2.0$ (a), $\alpha = -1.0$ (d) and $\alpha = 1.0$ (g) respectively. Susceptibility χ as a function of β for $\alpha = -2.0$ (b), $\alpha = -1.0$ (e) and $\alpha = 1.0$ (h). Average recovery rate at the steady state $\langle \mu(\infty) \rangle$ as a function of β for the corresponding α of the previous plots in (c), (f) and (i).

an optimal resource diffusion at $\alpha = -1.0$. Figure 2(c) shows that there are two bifurcation points β_s (triangles) and β_m (squares), and when $\alpha < \alpha_c$ there are two hysteresis loops in regions $[\beta_{\mathrm{per}}^I, \beta_s)$ and $[\beta_{\mathrm{per}}^{II}, \beta_m)$. When $\alpha > \alpha_c$ there is one hysteresis loop in region $[\beta_{\mathrm{per}}^I, \beta_m)$.

To further explore these results, we study the resource distribution (green circles) in layer $\mathcal{S}$ at the steady state when $\beta = (\beta_{\mathrm{inv}})_-$ for $\rho(0) = 0.01$, where $\beta = (\beta_{\mathrm{inv}})_-$ is the infection rate immediately below the threshold β_{inv} (see figure 3). When $\rho(0) = 0.99$ we see similar results. Here we denote $\omega(k^{\mathcal{S}}, \infty)$ the resource quantity of nodes with degree $k^{\mathcal{S}}$ at the steady state, where $k^{\mathcal{S}}$ is the degree of nodes in layer $\mathcal{S}$, and $\omega(k^{\mathcal{S}}, \infty)/N$ the scaled value of $\omega(k^{\mathcal{S}}, \infty)$. Note that $\omega(k^{\mathcal{S}}, \infty)$ is shortened to $\omega(k^{\mathcal{S}})$. In addition, to determine how the resource distribution in layer $\mathcal{S}$ influences the recovery of nodes in layer $\mathcal{C}$ at each value of parameter α, we examine how resources are distributed in nodes whose counterparts in layer $\mathcal{C}$ have $k^{\mathcal{C}}$ degrees, where $k^{\mathcal{C}}$ is the degree of nodes in layer $\mathcal{C}$. This allows us to observe the change trend of recovery rate with α.

Figure 3(a) shows that when $\alpha = -2.0$ resources move preferentially to low-degree nodes and $\omega(k^{\mathcal{S}})$ as expected decays rapidly with $k^{\mathcal{S}}$. In addition, most of the nodes in the two subnetworks with highly skewed degree distributions are low-degree and only a few are high-degree. Thus the counterparts of the high-degree nodes in layer $\mathcal{C}$ have a higher probability of being low-degree nodes in layer $\mathcal{S}$ because of the random correlation between the two layers. Thus most of the counterparts to the high-degree nodes in layer $\mathcal{C}$ have large values of $\omega(k^{\mathcal{S}})$ in layer S (yellow squares in figure 3(a)), i.e. most high-degree nodes in layer $\mathcal{C}$ have a high recovery rate that delays outbreaks of the
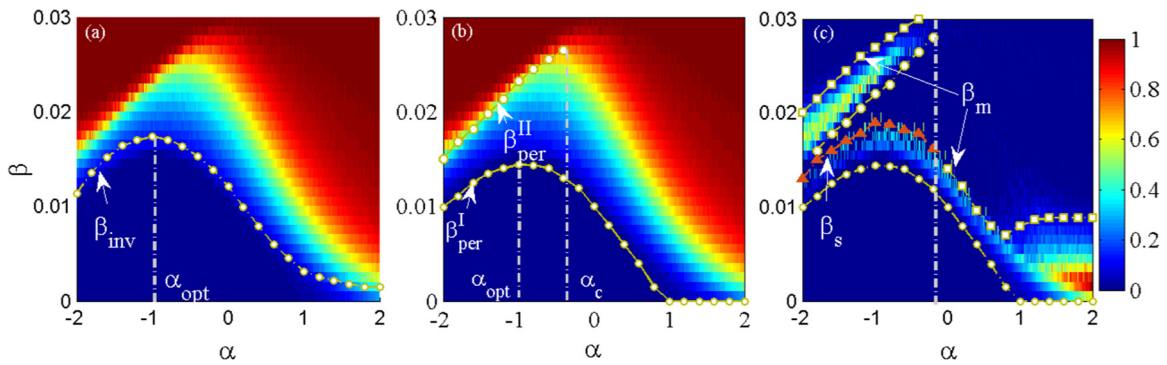
Figure 2. Dependence of $\rho(\infty)$ on β and α when $r = 0$. Color-coded values of epidemic size obtained from simulations for $\rho(0) = 0.01$ (a) and $\rho(0) = 0.99$ (b). (c) The difference between the value of $\rho(\infty)$ in (a) and (b). The yellow circles are the numerical prediction of the invasion threshold β_{inv} and the persistence threshold β_{per} respectively. Red triangles and yellow squares represent the two bifurcation points β_s and β_m respectively. The vertical dotted line in (a) indicates the location of the optimal value α_{opt}, and in (b) and (c) indicates the location of critical value α_c.

disease as β increases. When $\alpha = 1.0$ resources move preferentially toward high-degree nodes in layer $\mathcal{S}$ and agglomerate on high-degree nodes at the steady state. When there is a random correlation between the two layers, most high-degree nodes correspond to low-degree nodes in layer $\mathcal{C}$. Thus the resources of k-degree nodes in layer $\mathcal{S}$ increase with $k^{\mathcal{S}}$ (see figure 3(c)). In contrast, the $\omega(k^{\mathcal{S}})$ decreases sharply with $k^{\mathcal{C}}$, which indicates that the recovery rate of the high-degree nodes in layer $\mathcal{C}$ rapidly declines when β increases and resources decrease. This in turn increases the effective infection rate $\lambda = \beta/\langle\mu(\infty)\rangle$ in the system. Figure 2 shows that a severely skewed distribution of resources lowers the epidemic threshold and a large fraction of nodes when α is large, i.e. $\alpha = 1.0$.

When $\alpha = -1.0$, the diffusion of resources in layer $\mathcal{S}$ is less biased than when $\alpha = -2.0$ or $\alpha = 1.0$. We analyze equation (4) and find that although low-degree nodes still have a small advantage of acquiring resources, high-degree nodes can acquire approximately the same quantity of resource at each time step because they have more connections than low-degree nodes. Thus resources are distributed evenly for both high-degree and low-degree nodes (see figure 3(b)). When resource diffusion is optimal, all nodes in layer $\mathcal{C}$ have a rapid recovery rate (see figure 1(f)) that reduces the infection probability between each pair of susceptible and infected nodes. Here the disease is suppressed to the greatest extent. Figure 2 shows that the highest epidemic threshold β_{inv} (β_{per}) and lowest fraction of infected nodes $\rho(\infty)$ are obtained when resource diffusion is optimal, i.e. when $\alpha = -1.0$.

Our results play a practical guiding role in disease control. Specifically, when the infection rate of the disease is below the threshold, i.e. $\beta < \beta_{\mathrm{inv}}$ ($\beta < \beta_{\mathrm{per}}$ if $\rho(0)$ is large), the disease can not breakout globally. We find that strategy of resource diffusion has no significant effect on the disease spreading (see figure 2). While if $\beta > \beta_{\mathrm{inv}}$, the disease could breakout globally. Our findings indicate that the resources must be allocated properly to all the individuals in order to best suppress the disease spreading (see figures 2 and 3).
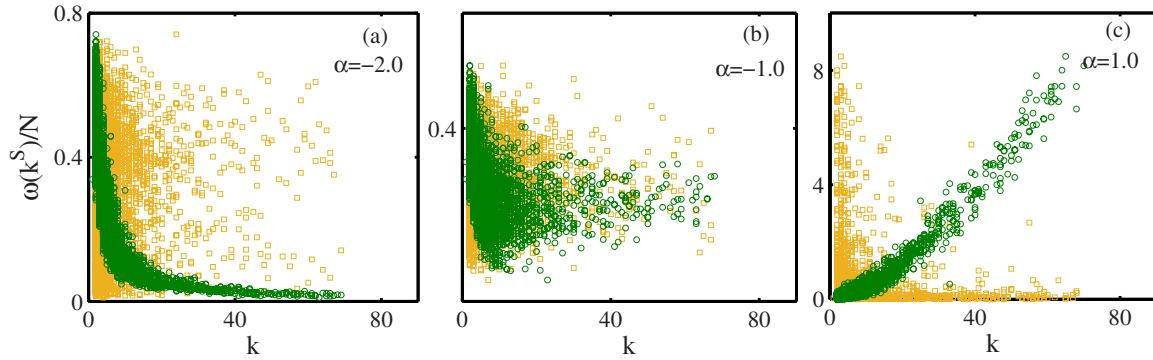
Figure 3. Scatter plots of resource quantity at $\beta = (\beta_{\text{inv}})_-$ for $\alpha = -2.0$ (a), $\alpha = -1.0$ (b) and $\alpha = 1.0$ (c) when the inter-layer degree correlation $r = 0$. The green circles represent scaled value of resource quantity $\omega(k^{\mathcal{S}})/N$ versus degree of nodes $k^{\mathcal{S}}$, and the yellow squares represent $\omega(k^{\mathcal{S}})/N$ versus the degree of the counterpart nodes $k^{\mathcal{C}}$. The initial fraction of infected nodes is set to $\rho(0) = 0.01$.

4. Effect of inter-layer degree correlations on spreading dynamics

There are extensive interlayer correlations in real-world multiplex systems [51, 52]. In social networks, for example, an individual with many daily face-to-face contacts with colleagues tends to also have many social network contacts [35]. In transportation networks, hub airports tend to correlate with hub rapid transit stations [53]. We here investigate how the degree correlations between the two layers impact the process of resource diffusion and the dynamics of disease spreading. To construct a double-layer correlated network with an adjustable degree of inter-layer correlation, we first generate two subnetworks of the same size $N = 5000$ and the same power exponent $\gamma = 2.2$ with a maximum positive or maximum negative correlation. We then rematch each pair of counterpart nodes with a probability q. Thus the interlayer correlation after rematching becomes [37, 38]

$$r = \mid 1 - q \mid . \tag{6}$$

When the two layers are initially at maximum positive correlation $r \geqslant 0$, otherwise $r \leqslant 0$.

Figures 4 and 5 show $\rho(\infty)$ as a function of β when there is a large negative inter-layer correlation, i.e. $r = -0.8$, and large positive correlation, i.e. $r = 0.8$. When $r = -0.8$, the results of three typical values $\alpha = -1.5$, 0, and 1.0 for $\rho(0) = 0.01$ (red circles) and $\rho(0) = 0.99$ (blue squares) are displayed. When $\alpha = -1.5$, $\rho(\infty)$ has two phase transitions for $\rho(0) = 0.99$ and two hysteresis loops (see figures 4(a) and (b)). When $\alpha = 0$ and $\alpha = 1.0$, $\rho(\infty)$ has one phase transition and a single hysteresis loop. The peak values of χ in figures 4(b), (d), and (f) are the transition points for $\rho(0) = 0.01$ (red lines) and $\rho(0) = 0.99$ (blue squares).

Figure 5 shows the four typical values $\alpha = -2.0$, -0.5, 0, and 1.0 when $r = 0.8$. We find that when α increases, the phase transition of $\rho(\infty)$ changes from multiple continuous ($\alpha = -2.0$, see figure 5(a)) to discontinuous (figure 5(c)) to hybrid (inset of figure 5(c)). Eventually it returns to being multiple continuous (figure 5(e)). In addition, when $\alpha = 1.0$ the first threshold disappears when $\rho(0) = 0.99$. Later in the Appendix section, we will use a finite-size scaling analysis to demonstrate the discontinuous

increase of $\rho(\infty)$ [54–56]. In addition, qualitative explanations for the hybrid phase transition will be made. Note that, unlike when $r = 0$ or $r = -0.8$, there is single hysteresis loop for all values of α. We can obtain the same explanation for the hysteresis loops by analyzing the ensemble average recovery rate $\langle \mu(\infty) \rangle$ as a function of β, similar to when $r = 0$.

To determine how preferential resource diffusion affects the dynamics of epidemic spreading when there is interlayer degree correlation, we use two-parameter (α, β) phase diagrams for $r = -0.8$ and $r = 0.8$ (see figure 6). The colors used in the figures are the values of $\rho(\infty)$. We set the initial fraction of seeds at $\rho(0) = 0.01$ in figures 6(a) and (d) and at $\rho(0) = 0.99$ in figures 6(b) and (e) at $r = -0.8$ and $r = 0.8$, respectively. Figures 6(c) and (f) show the differences between $\rho(\infty)$ in figures 6(a) and (b) and in figures 6(c) and (d). Note that there are optimal values of α, i.e. $\alpha_{\mathrm{opt}} \simeq -1.5$ for $r = -0.8$ (see figures 6(a) and (b)) and $\alpha_{\mathrm{opt}} \simeq -0.5$ for $r = 0.8$ (see figures 6(d) and (e)). Around α_{opt} the disease is maximally suppressed, the value of β_{inv} (β_{per}) reaches a maximum, and $\rho(\infty)$ a minimum (see figures 6(a)–(d) for $r = -0.8$ and $r = 0.8$, respectively). Similar to when $r = 0$, when $r = -0.8$ and $\rho(0) = 0.99$ there is an α_c critical value. When $\alpha < \alpha_c$ there are two phase transitions of $\rho(\infty)$ with two transition points β_{per}^{I} and $\beta_{\mathrm{per}}^{II}$ (see figure 6(b)). When $\alpha > \alpha_c$ the transition of $\rho(\infty)$ becomes single-phase. When $\rho(0) = 0.01$ there is a single phase transition of $\rho(\infty)$ (see figure 6(a)).

We obtain thresholds from susceptibility χ. Figure 6(c) shows that when $\alpha < \alpha_c$ there are two bifurcations, β_s (triangles) and β_m (squares) where $\beta_s < \beta_m$. There are two hysteresis loops in regions $[\beta_{\mathrm{per}}^{I}, \beta_s)$ and $[\beta_{\mathrm{per}}^{II}, \beta_m)$. When $\alpha > \alpha_c$ there is one hysteresis loop in region $[\beta_{\mathrm{per}}^{I}, \beta_m)$. We find multiple phase transitions when $r = 0.8$ and when α is far from α_{opt}, i.e. $\alpha = -1.0$ or $\alpha = 1.0$. Note that for simplicity we display only the first invasion threshold β_{inv}^{I} and the first persistence threshold β_{per}^{I} in figures 6(d) and (e) (circles), which we obtain from susceptibility measurement χ. When α approaches α_{opt}, i.e. when $\alpha = -0.5$, the value of $\rho(\infty)$ jumps from zero to a high value. In addition, the difference in $\rho(\infty)$ values in figures 6(d) and (e) indicates the single hysteresis region $(\beta_{\mathrm{per}}^{I}, \beta_m)$ (white circles and white squares in figure 6(f)).

To explain the optimization, we examine the resource distribution of nodes in layer $\mathcal{S}$ and how resources are distributed on those nodes whose counterparts in layer $\mathcal{C}$ have $k^{\mathcal{C}}$ degrees when $\beta = (\beta_{\mathrm{inv}}^{I})_-$ ($\beta = (\beta_{\mathrm{inv}})_-$ if it is a single phase transition). Thus we obtain the scatter plots of $\omega(k^{\mathcal{S}})/N$ versus $k^{\mathcal{S}}$ (green circles) and $\omega(k^{\mathcal{S}})/N$ versus $k^{\mathcal{C}}$ (yellow squares). We obtain results similar to those when $\rho(0) = 0.99$.

Figures 7(a)–(c) show resource distributions for $\alpha = -1.5$, 0.0, and 1.0, respectively for $r = -0.8$. Note that when $\alpha = -1.5$ the probability that resources move to low-degree nodes in layer $\mathcal{S}$ is high. Figure 7(a) shows that $\omega(k^{\mathcal{S}})/N$ decreases sharply when $k^{\mathcal{S}}$ in layer $\mathcal{S}$ increases (green circles). In addition, when the correlation between the two layers is negative, high-degree nodes in layer $\mathcal{C}$ correlate with low-degree nodes. Because low-degree nodes are more numerous in a heterogeneous network, most low-degree nodes in layer $\mathcal{C}$ still have low-degree counterparts. Thus both high-degree and low-degree nodes in layer $\mathcal{C}$ can rapidly recover because there are adequate resources supplied by their counterparts in layer $\mathcal{S}$ (yellow squares in figure 7(a)). When this is the case, the disease is effectively constrained (see figure 6(a)).
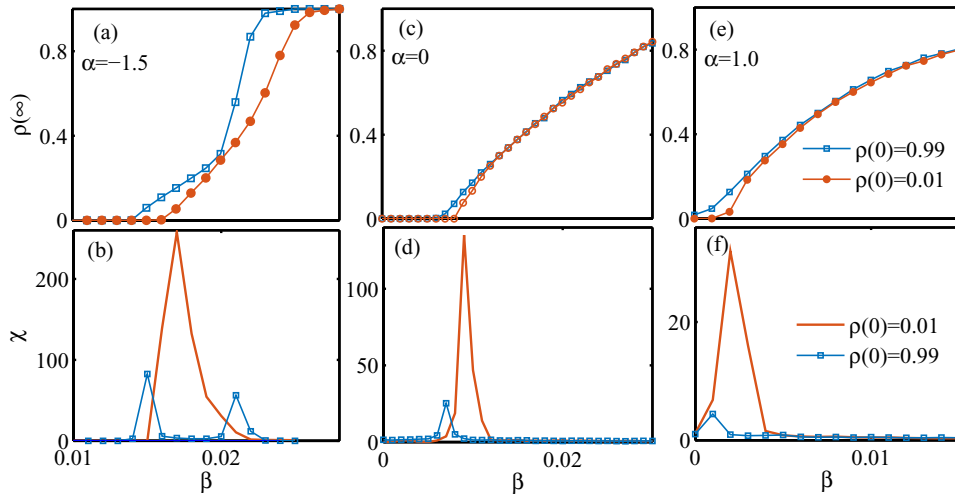
Figure 4. Influence of preferential resource diffusion on disease spreading when degree of inter-layer correlation is $r = -0.8$. $\rho(\infty)$ as a function of β for $\alpha = -1.5$ (a), $\alpha = 0$ (c) and $\alpha = 1.0$ (e) respectively, Initial condition is set to $\rho(0) = 0.01$ (red circles) and $\rho(0) = 0.99$ (blue squares) respectively in the figures. Susceptibility measure χ as a function of β for $\alpha = -1.5$ (b), $\alpha = 0$ (d) and $\alpha = 1.0$ (f) respectively.
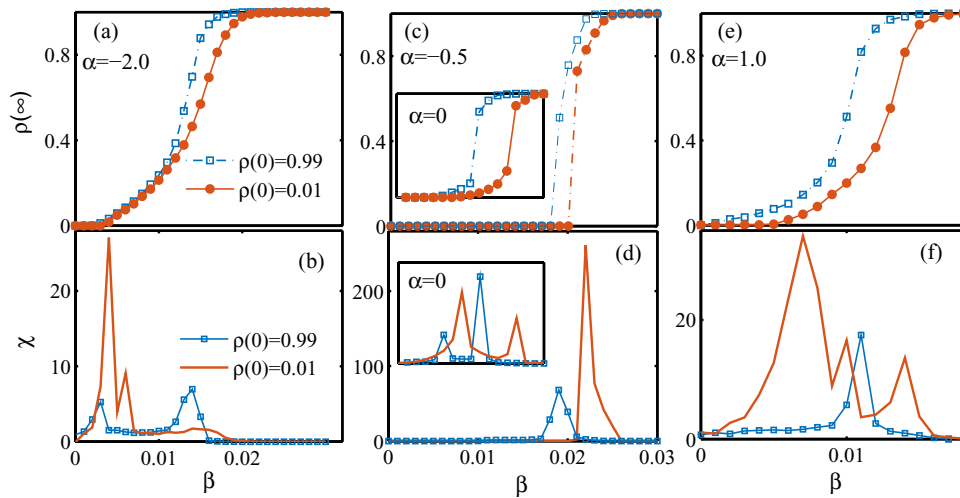
Figure 5. Influence of preferential resource diffusion on disease spreading when degree of inter-layer correlation $r = 0.8$. $\rho(\infty)$ as a function of β for $\alpha = -2.0$ (a), $\alpha = -1.0$ (c) and $\alpha = 1.0$ (e) respectively. Inset of (b) is $\rho(\infty)$ versus β for $\alpha = 0$, Initial condition is set to $\rho(0) = 0.01$ (red circles) and $\rho(0) = 0.99$ (blue squares) respectively in the figures. Susceptibility measure χ as a function of β for $\alpha = -2.0$ (b), $\alpha = -1.0$ (d) and $\alpha = 1.0$ (f) respectively. Inset of (d) is χ versus β for $\alpha = 0$.

While, when $\alpha = 0$ and $\alpha = 1.0$, resources move preferentially to the few high-degree nodes in layer S and low-degree nodes receive little (green circles in figures 7(b) and (c)). When β increases, the recovery rate of high-degree nodes in layer C rapidly decreases because they cannot receive resources from their counterparts (yellow circles in figures 7(b) and (c)) and the disease is not constrained. Thus we see a small threshold and a large $\rho(\infty)$ when resources move preferentially to high-degree nodes in layer S.
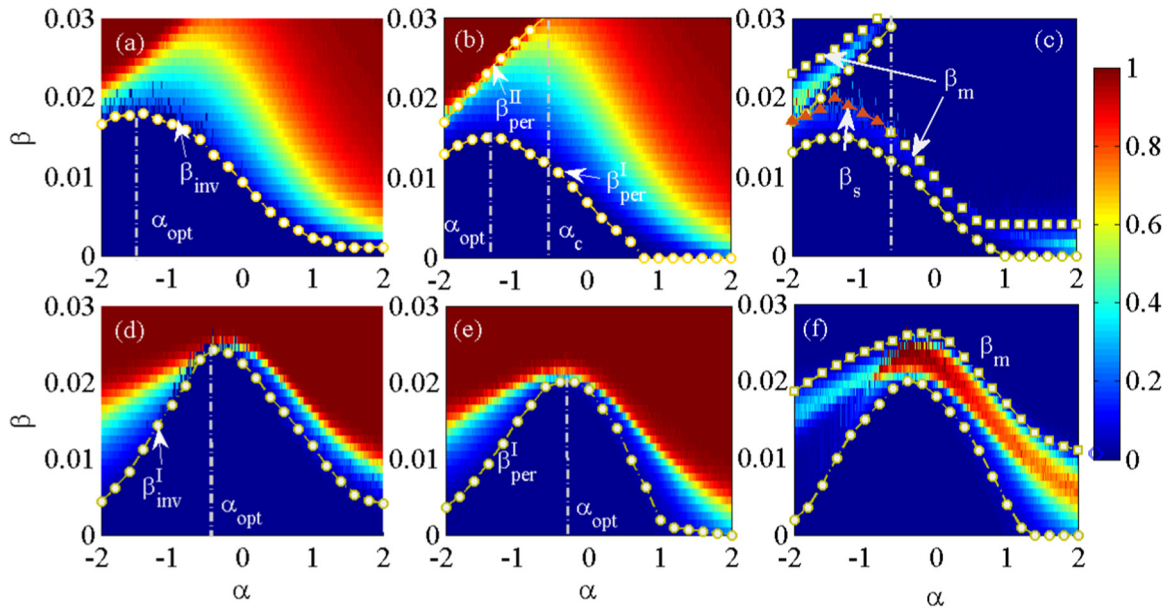
Figure 6. Dependence of $\rho(\infty)$ on β and α when $r = -0.8$ (the first row) and $r = 0.8$ (the second row). Color-coded values of epidemic size obtained from simulations for $\rho(0) = 0.01$ (a), (d) and $\rho(0) = 0.99$ (b), (e). The difference of the value of $\rho(\infty)$ in (a), (b) and (d), (e). The yellow circles are the numerical prediction of the invasion threshold β_{inv} and the persistence threshold β_{per} respectively, which are obtained from the peaks of the susceptibility measure χ. Triangles and squares in (c), and (f) represent the bifurcation points β_s and β_m respectively. The vertical dashed lines in (a) and (d) indicate the location of the optimal value α_{opt}, and in (b), (c) indicate the location of critical value α_c.

When $r = 0.8$ the degrees of nodes correlated positively between the two layers, to constrain disease spreading the recovery rate of both high and low degree nodes in layer $\mathcal{C}$ should maintain a high threshold. To achieve this, resources must diffuse properly to high-degree nodes in layer $\mathcal{S}$ (i.e. $\alpha \simeq -0.5$) in a positive correlation between the two layers. Thus when $\alpha = \alpha_{\mathrm{opt}} \simeq -0.5$ there is a maximum threshold value and a minimum $\rho(\infty)$ value when β is fixed.

Figure 7(f) shows that when resources move only to high-degree nodes in layer $\mathcal{S}$, i.e. when $\alpha = 1.0$, there are no resources for the low-degree nodes in layer $\mathcal{S}$. Figure 7(d) shows that when resources move only to low-degree nodes, there are none for the high-degree nodes. In both of these extreme conditions, the node recovery rate in layer $\mathcal{C}$ declines rapidly as β increases, which causes an earlier outbreak of disease (see figures 6(d) and (e)).

The results indicate that the inter-layer correlation of a social system can significantly influence the human behavior and the public policy in controlling the disease spreading. Specifically, if a social system has negative inter-layer correlation (namely the individuals in the system who have large connections in the virtual social networks tend to have few connections in the physical contact network), resources should be properly diffuse to those individuals who have small connections in the social layer. Thus the people they have frequent physical contact can get more resources and better treatment if they get infected. In contrary, if a social system has positive inter-layer correlation, then the
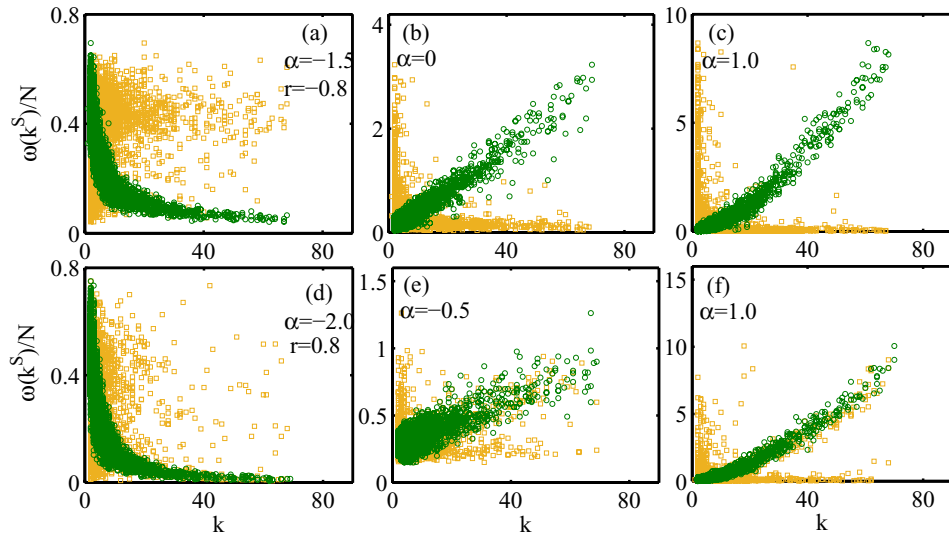
Figure 7. Scatter plots of resource quantity at $\beta = (\beta_{\text{inv}}^{I})_{-}$ when the inter-layer degree correlation $r = -0.8$ (a)–(c), and $r = 0.8$ (d)–(f). The green circles represent scaled resource quantity $\omega(k^{\mathcal{S}})/N$ versus $k^{\mathcal{S}}$, and the yellow squares represent $\omega(k^{\mathcal{S}})/N$ versus $k^{\mathcal{C}}$. The initial fraction of infected nodes is set to $\rho(0) = 0.01$.

resources should diffuse preferentially to the individuals who have large connections in the social networks. Since in a network with positive inter-layer correlations, an individual has large connections in the social network tends to have large physical contacts in the contact networks.

Figure 8(a) plots the value of the first invasion threshold β_{inv}^{I} as a function of α for three typical degree correlations, $r = -0.8$ (gray circles), $r = 0$ (green squares), and $r = 0.8$ (red triangles), with an initial condition $\rho(0) = 0.01$. When $\rho(0) = 0.99$ the results are similar. Note that the three curves cross at $\alpha = -1.0$ (point C in figure 8(a)). When $\alpha < -1$, β_{inv}^{I} decreases with r, but when $\alpha > -1$, β_{inv}^{I} increases with r. When $\alpha < -1$, resources move preferentially to low-degree nodes in layer S. To suppress the spreading, the nodes in layer S must supply enough resources to high-degree nodes in layer C. Thus negative interlayer correlation enhances the disease suppression. In contrast, when $\alpha > -1$ high-degree nodes add resources in layer S. To constrain these high-degree nodes we must have high-degree counterparts in layer C. Thus we increase β_{inv}^{I} with r.

Finally we explore the relationship among the optimal values of the bias parameter α_{opt} at which the disease is maximally controlled. Figure 8(b) shows α_{opt} as a function of r. Note that the value of α_{opt} increases monotonically with r because, with the increase of the interlayer correlation, the probability that the large degree nodes in layer $\mathcal{S}$ have counterparts with large degrees also increases. To protect the large degree nodes in layer $\mathcal{C}$, resources in layer $\mathcal{S}$ must diffuse preferentially to large degree nodes. Thus α_{opt} increases with r.
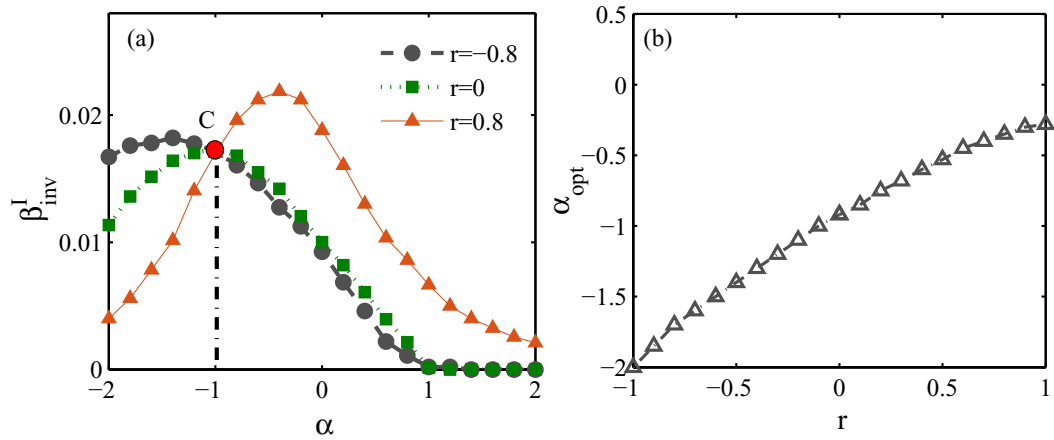
Figure 8. The value of the first invasion threshold β_{inv}^{I} as a function of the bias parameter α for $r = -0.8$ (gray circles), $r = 0$ (green squares) and $r = 0.8$ (red triangles) (a). Optimal bias parameter α_{opt} as a function of inter-layer correlation r (b). Each symbol in (a) is obtained from the susceptibility measure. Red circle at $\alpha = -1.0$ is the cross point of the three lines. Here the initial condition is set to $\rho(0) = 0.01$.

5. Discussion and conclusions

We have explored how preferential resource diffusion affects the dynamics of disease spreading in correlated multiplex networks. Using extensive simulations we found that preferential resource diffusion can change the phase transition in $\rho(\infty)$, i.e, when the degree of interlayer correlation r is below a critical value, the transition of $\rho(\infty)$ with $\rho(0) = 0.99$ changes from two continuous phase transitions to one single phase transition as the controlling parameter α increases. We found two hysteresis loops accompanied by two phase transitions and one single hysteresis loop accompanied by one single phase transition of $\rho(\infty)$. When r is above the critical value, the phase transition of $\rho(\infty)$ changes with α from multiple to discontinuous, and then becomes hybrid. There is an optimal resource diffusion at each fixed value of r. When the diffusion of resources is optimal the threshold reaches a maximum and the disease can be maximally suppressed.

The results of our model indicate that the diffusion of resources in our daily lives could have significant influence in suppressing disease spreading, which can help policy makers to make an optimal strategy through properly controlling the flow of resources in social systems in order to effectively suppress outbreaks of the disease. Specifically, according to the network structure of the social circle, we can adopt distinct resource diffusion strategies to best suppress disease spreading. If there is no inter-layer correlation between the social layer and physical contact layer, the resources should diffuse uniformly in the social layer of the individuals. Otherwise, if there is a negative correlation between the two layers of the network, we should appropriately control the diffusion of resources to the individuals who have small connections in the social network. Last, if there is a positive correlation between the two layers, resources should diffuse appropriately to those individuals who have more connections in the social networks.
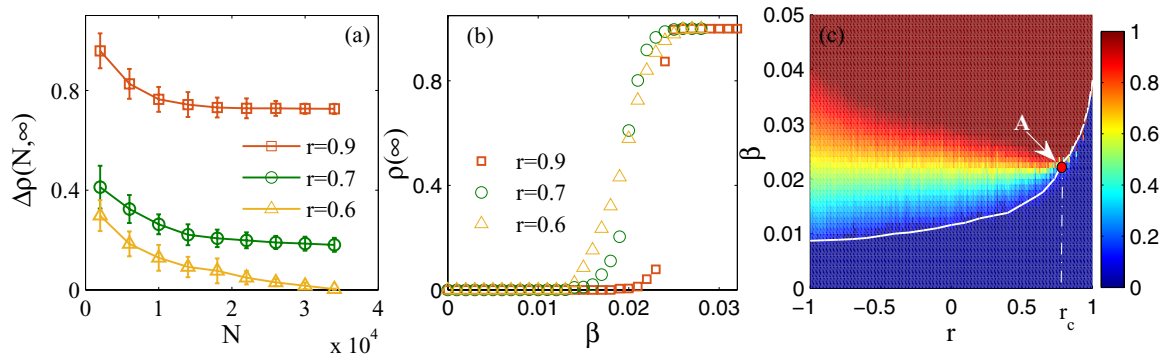
Figure A1. Results of finite-size scaling analysis for the discontinuous increase of $\rho(\infty)$. (a) Increase of infected density at the steady state $\Delta\rho(N,\infty)$ as a function of network size N for $r=0.9$ (red squares), $r=0.7$ (green circles) and $r=0.6$ (yellow triangles). (b) Infected density $\rho(\infty)$ as a function of β for $r=0.9$ (red squares), $r=0.7$ (green circles) and $r=0.6$ (yellow triangles) respectively. (c) Dependence of $\rho(\infty)$ on r and β. Color-coded values of $\rho(\infty)$ obtained from simulations with initial condition $\rho(0)=0.01$. Point A is a triple point and the corresponding r is the critical value r_c. White line represents the first epidemic threshold β_{inv}^I that are obtained from the peaks of χ. The bias parameter is set to $\alpha=0$.

Because the model is complex we have not yet developed theoretical solutions, and thus theoretically obtaining an optimal solution α_{opt} would be an interesting and important objective for future research. Previous studies indicated that the degree correlation in the layer has great influence on both dynamics of the networks [58] and dynamics on the networks [59], thus it may also influence the strategy of the resource diffusion. It would be interesting to discuss the coupling of the resource diffusion and disease spreading when there is degree correlation in the two layers.

Acknowledgments

Appendix

In this section, we use finite-size scaling analysis to examine the discontinuous increase of $\rho(\infty)$ when α approaches α_{opt} and the two network layers are positively correlated. We define $\rho(N,\infty)$ the fraction of infected nodes at the steady state for a network with N nodes and $\Delta\rho(N,\infty)$ the maximum increase of $\rho(N,\infty)$ during an infinitely small increase of β, which is expressed
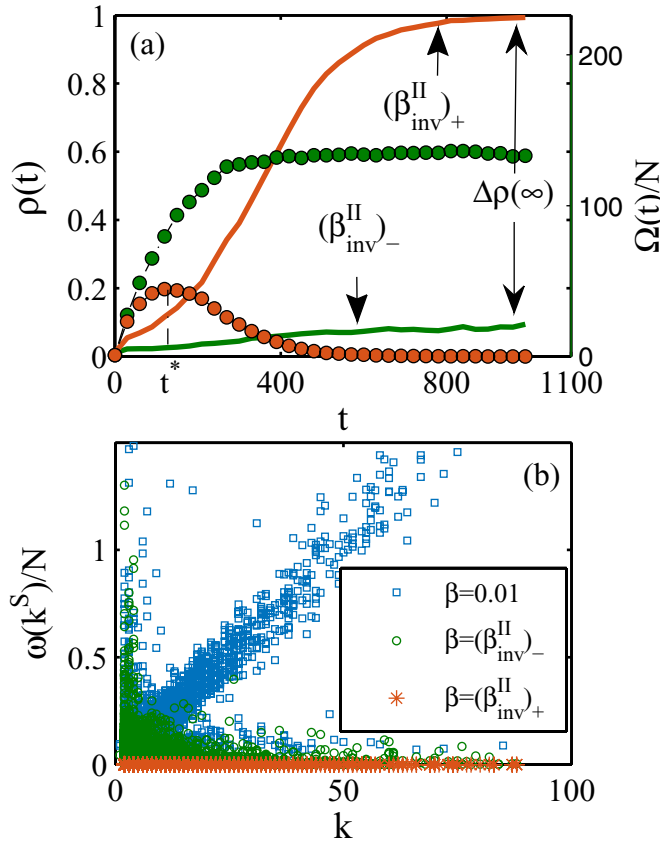
Figure A2. Analysis of the hybrid phase transition. (a) The left vertical axis shows the time evolution of $\rho(t)$ when β is just below the second threshold $(\beta_{\mathrm{inv}}^{II})_-$ (the lower green line) and just over $(\beta_{\mathrm{inv}}^{II})_+$ (the upper red line). The right vertical axis shows the time evolution of scaled total resources of all nodes $\Omega(t)/N$ for $(\beta_{\mathrm{inv}}^{II})_-$ (the upper green circles) and $(\beta_{\mathrm{inv}}^{II})_+$ (the lower red circles). (b) Resource distribution in layer S for $\beta = 0.01$ (blue squares), $(\beta_{\mathrm{inv}}^{II})_-$ (green circles) and $(\beta_{\mathrm{inv}}^{II})_+$ (red stars).

$$\Delta\rho(N,\infty) = \max_{\beta \in [0,1]}\{\rho(N,\infty,\beta+\Delta\beta) - \rho(N,\infty,\beta)\}, \tag{A.1}$$

where $\Delta\beta$ is an infinitesimal increment of β, set at $\Delta\beta = 0.001$ in our simulations, and $\rho(N,\infty,\beta)$ is the fraction of infected nodes at steady state when infection rate is β. When

$$\lim_{N \to \infty} \Delta\rho(N,\infty) > 0.0, \tag{A.2}$$

there is a discontinuous increase in $\rho(\infty)$ [53, 57]. Note that we use $\alpha = 0$ for the finite-size scaling analysis. Figure A1(a) shows $\Delta\rho(N,\infty)$ as a function of N when $\alpha = 0.6$ (orange triangles), $\alpha = 0.7$ (green circles), and $\alpha = 0.9$ (red squares). Note that when $\alpha = 0.6$, $\Delta\rho(N,\infty)$ converges to 0 asymptotically. When $\alpha = 0.7$ and $\alpha = 0.9$, $\Delta\rho(N,\infty)$ asymptotically converges to a positive constant.

Figure A1(b) shows $\rho(\infty)$ as a function of β when $\rho(0) = 0.01$ for three typical values of interlayer correlation $r = 0.6$, $r = 0.7$, and $r = 0.9$ in a network of size $N = 10000$. Note that when $r = 0.6$, $\rho(\infty)$ increases continuously with β. When $r = 0.7$ and $r = 0.9$,

$\rho(\infty)$ first increases slowly and continuously at β_{inv}^{I}, and then jumps discontinuously at $\beta_{\mathrm{inv}}^{II}$, all of which are characteristics of a hybrid phase transition.

We next use extensive simulations to obtain the phase diagram of $\rho(\infty)$ in the two-parameter (r, β) plane with an initial condition $\rho(0) = 0.01$ when $\alpha = 0$. When $\rho(0) = 0.99$ the results are similar. Figure A1(c) shows that when the two layers are negatively correlated ($r < 0$), $\rho(\infty)$ increases continuously with β. When $r > 0$, there is a critical value point r_c (point A in figure A1(c)). When $r \geqslant r_c$ there is a discontinuous change of $\rho(\infty)$ at the threshold. Note also that the epidemic threshold increases with r (see white line in figure A1(c)).

To explain the hybrid discontinuous phase transition, we plot the time evolution of total resources $\Omega(t)$ and infected fraction $\rho(t)$ with the initial condition $\rho(0) = 0.01$ for $r = 0.9$ when $\alpha = 0$ (see figure A2(a)). When $\rho(0) = 0.99$ the results are similar. Figure A2(b) shows the corresponding resource distribution at the steady state. When β is immediately below $(\beta_{\mathrm{inv}}^{II})_{-}$, the scaled value of the total resources $\Omega(t)/N$ abruptly increases at the early stage of the diffusion process (green circles in figure A2(a)) because almost all nodes in layer $\mathcal{C}$ are healthy and resources are constantly generated by the corresponding nodes in layer $\mathcal{S}$. After a longer period of time $t > 300$ the system enters a steady state, and fluctuations stay within a small range (upper green circles). Here the resources of high-degree nodes are rapidly consumed, and the resource level for low-degree nodes remains high (see figure A2(b)) indicating that the disease is localized around the high-degree nodes. We thus learn that before $\beta_{\mathrm{inv}}^{II}$ the system changes from a disease-free absorbing phase to a locally active phase (in which $\rho(\infty)$ reaches a finite small value) at β_{inv}^{I} (green line in figure A2(a)). For the sake of comparison, figure A2(b) shows a plot of the resource distribution when $\beta = 0.01$.

When $\beta = (\beta_{\mathrm{inv}}^{II})_{+}$, the value of $\Omega(t)/N$ rapidly increases as the disease spreads from the local area of the seeds (red circles in figure A2(a)). As t increases $\rho(t)$ slowly increases and $\Omega(t)/N$ reaches a peak value at a crossover time t^{*}. After t^{*}, $\Omega(t)/N$ drops rapidly, indicating that the newly-generated node resources in layer $\mathcal{S}$ are not sufficient to recover the infected nodes in layer $\mathcal{C}$. The recovery rate of the infected nodes then declines as resources decrease, which induces an increase in the infection rate of the disease, especially in the hub nodes. Thus as the infection rate increases, the resources available in layer $\mathcal{S}$ further decrease and the node recovery rate in layer $\mathcal{C}$ decreases. Then a cascading effect appears that sharply increases $\rho(t)$ from a small finite value to a value near 1.0 (red line in figure A2(a)). Figure A2(a) shows $\Delta\rho(\infty)$, which is the increase of $\rho(\infty)$ when β increases from $(\beta_{\mathrm{inv}}^{II})_{-}$ to $(\beta_{\mathrm{inv}}^{II})_{+}$. This indicates a discontinuous jump in $\rho(\infty)$. Figure A2(b) shows that all resources of all nodes in the network have been consumed, in contrast to when $(\beta_{\mathrm{inv}}^{II})_{-}$.

References

[1] Pastor-Satorras R, Castellano C, Van Mieghem P and Vespignani A 2015 *Rev. Mod. Phys.* **87** 925
[2] Pastor-Satorras R and Vespignani A 2001 *Phys. Rev. Lett.* **86** 3200
[3] Gómez S, Arenas A, Borge-Holthoefer J, Meloni S and Moreno Y 2010 *Europhys. Lett.* **89** 38009
[4] Givan O, Schwartz N, Cygelberg A and Stone L 2011 *J. Theor. Biol.* **288** 21–8
[5] Wang W, Tang M, Stanley H E and Braunstein L A 2016 *Rep. Prog. Phys.* **80** 036603
[6] Moreno Y, Nekovee M and Pacheco A F 2004 *Phys. Rev.* E **69** 066130
[7] Trpevski D, Tang W K and Kocarev L 2010 *Phys. Rev.* E **81** 056102

[8] Newman M E, Forrest S and Balthrop J 2002 *Phys. Rev.* E **66** 035101
[9] Balthrop J, Forrest S, Newman M E and Williamson M M 2004 *Science* **304** 527–9
[10] Lau S K *et al* 2005 *Proc. Natl Acad. Sci. USA* **102** 14040–5
[11] Pastor-Satorras R and Vespignani A 2002 *Phys. Rev.* E **65** 036104
[12] Alvarez-Zuzek L G, Buono C and Braunstein L A 2015 *J. Phys.: Conf. Ser.* **640** 012007
[13] Dezső Z and Barabási A L 2002 *Phys. Rev.* E **65** 055103
[14] Holme P, Kim B J, Yoon C N and Han S K 2002 *Phys. Rev.* E **65** 056109
[15] Buono C and Braunstein L A 2015 *Europhys. Lett.* **109** 26001
[16] Cohen R, Havlin S and Ben-Avraham D 2003 *Phys. Rev. Lett.* **91** 247901
[17] Chen Y, Paul G, Havlin S, Liljeros F and Stanley H E 2008 *Phys. Rev. Lett.* **101** 058701
[18] Clusella P, Grassberger P, Pérez-Reche F J and Politi A 2016 *Phys. Rev. Lett.* **117** 208301
[19] Funk S, Gilad E, Watkins C and Jansen V A 2009 *Proc. Natl Acad. Sci. USA* **106** 6872–7
[20] Ruan Z, Tang M and Liu Z 2012 *Phys. Rev.* E **86** 036117
[21] Granell C, Gómez S and Arenas A 2013 *Phys. Rev. Lett.* **111** 128701
[22] Tragler G, Caulkins J P and Feichtinger G 2001 *Oper. Res.* **49** 352–62
[23] Lokhov A Y and Saad D 2017 *Proc. Natl Acad. Sci. USA* **114** 201614694
[24] Chen H, Li G, Zhang H and Hou Z 2017 (arXiv:1702.08444)
[25] Team W E R 2015 *New Engl. J. Med.* **372** 584
[26] Gallup J L and Sachs J D 2001 *AM. J. Trop. Med. Hyg.* **64** 85–96
[27] Berke P R, Kartez J and Wenger D 1993 *Disasters* **17** 93–109
[28] Böttcher L, Woolley-Meza O, Araújo N A, Herrmann H J and Helbing D 2015 *Sci. Rep.* **5** 16571
[29] Böttcher L, Woolley-Meza O, Goles E, Helbing D and Herrmann H 2016 *Phys. Rev.* E **93** 042315
[30] Chen X L, Zhou T, Feng L, Yang C, Wang M, Fan X and Hu Y 2016 (arXiv:1611.00212)
[31] Chen X L, Wang R J, Tang M, Cai S M, Stanley H E and Braunstein L A 2018 *New J. Phys.* **20** 013007
[32] Perc M 2014 *J. R. Soc. Interface* **11** 20140378
[33] Mucha P J, Richardson T, Macon K, Porter M A and Onnela J P 2010 *Science* **328** 876–8
[34] De Domenico M, Granell C, Porter M A and Arenas A 2016 *Nat. Phys.* **12** 901–6
[35] Szell M, Lambiotte R and Thurner S 2010 *Proc. Natl Acad. Sci. USA* **107** 13636–41
[36] Catanzaro M, Boguñá M and Pastor-Satorras R 2005 *Phys. Rev.* E **71** 027103
[37] Lee K M, Kim J Y, Cho W K, Goh K I and Kim I 2012 *New J. Phys.* **14** 033027
[38] Wang W, Tang M, Yang H, Do Y, Lai Y C and Lee G 2014 *Sci. Rep.* **4** 5097
[39] Viswanath B, Mislove A, Cha M and Gummadi K P 2009 On the evolution of user interaction in facebook *Proc. of the 2nd ACM Workshop on Online Social Networks* (ACM) pp 37–42
[40] Adamic L A and Huberman B A 2000 *Science* **287** 2115
[41] Molloy M and Reed B 1995 *Random Struct. Algorithms* **6** 161–80
[42] Boguná M, Pastor-Satorras R and Vespignani A 2004 *Euro. Phys. J.* B **38** 205–9
[43] Cohen R, Havlin S and Ben-Avraham D 2002 *Handbook of Graphs and Networks* (New York: Wiley-VCH) ch 4
[44] Binder K *et al* 1993 *Comput. Phys.* **7** 156–7
[45] Ferreira S C, Castellano C and Pastor-Satorras R 2012 *Phys. Rev.* E **86** 041125
[46] Colomer-de Simón P and Boguñá M 2014 *Phys. Rev.* X **4** 041020
[47] Chen W, Schröder M, D'Souza R M, Sornette D and Nagler J 2014 *Phys. Rev. Lett.* **112** 155701
[48] Majdandzic A, Podobnik B, Buldyrev S V, Kenett D Y, Havlin S and Stanley H E 2014 *Nat. Phys.* **10** 34
[49] Majdandzic A, Braunstein L A, Curme C, Vodenska I, Levy-Carciente S, Stanley H E and Havlin S 2016 *Nat. Commun.* **7** 10850
[50] Gross T, D'Lima C J D and Blasius B 2006 *Phys. Rev. Lett.* **96** 208701
[51] Kivelä M, Arenas A, Barthelemy M, Gleeson J P, Moreno Y and Porter M A 2014 *J. Complex Netw.* **2** 203–71
[52] Valdez L D, Macri P A and Stanley H Eand Braunstein L A 2013 *Phys. Rev.* E **88** 50803
[53] Radicchi F 2015 *Nat. Phys.* **11** 597–602
[54] Newman M and Barkema G 1999 *Monte Carlo Methods in Statistical Physics* (New York: Oxford University Press) ch 1–4
[55] Radicchi F and Fortunato S 2010 *Phys. Rev.* E **81** 036110
[56] Chen X L, Yang C, Zhong L and Tang M 2016 *Chaos* **26** 083114
[57] Nagler J, Levina A and Timme M 2011 *Nat. Phys.* **7** 265
[58] Noh J D 2007 *Phys. Rev.* E **76** 026116
[59] Boguná M, Pastor-Satorras R and Vespignani A 2003 *Phys. Rev. Lett.* **90** 028701